

Feasibility of intrafraction whole body motion tracking for total marrow irradiation

Manju Sharma
Troy Dos Santos
Nikolaos P. Papanikolopoulos
Susanta Kumar Hui

Feasibility of intrafraction whole body motion tracking for total marrow irradiation

Manju Sharma,^a Troy Dos Santos,^a Nikolaos P. Papanikolopoulos,^{b,c} and Susanta Kumar Hui^{a,c,d}

^aUniversity of Minnesota Medical School, Department of Therapeutic Radiology–Radiation Oncology, MMC 494–420

Delaware Street SE, Minneapolis, Minnesota 55455

^bUniversity of Minnesota Medical School, Department of Computer Science and Engineering, MMC 494–420

Delaware Street SE, Minneapolis, Minnesota 55455

^cUniversity of Minnesota Medical School, Biomedical Engineering, MMC 494–420 Delaware Street SE, Minneapolis,

Minnesota 55455

^dUniversity of Minnesota Medical School, Biophysical Sciences and Medical Physics MMC 494–420 Delaware Street

SE, Minneapolis, Minnesota 55455

Abstract. With image-guided tomotherapy, highly targeted total marrow irradiation (TMI) has become a feasible alternative to conventional total body irradiation. Problem: The uncertainties in patient localization and intrafraction motion of the whole body during hour-long TMI treatment may pose a risk to the safety and accuracy of targeted radiation treatment. The feasibility of near-infrared markers and optical tracking system (OTS) is accessed along with a megavoltage scanning system of tomotherapy. Three near-infrared markers placed on the face of a RANDO phantom are used to evaluate the capability of OTS in measuring changes in the markers' positions as the RANDO is moved in the translational direction. The OTS is also employed to determine breathing motion related changes in the position of 16 markers placed on the chest surface of human volunteers. The maximum uncertainty in locating marker position with the OTS is 1.5 mm. In the case of normal and deep breathing motion, the maximum marker position change is observed in anterior–posterior direction with the respective values of 4 and 12 mm. The OTS is able to measure surface changes due to breathing motion. The OTS may be optimized to monitor whole body motion during TMI to increase the accuracy of treatment delivery and reduce the radiation dose to the lungs. © 2011 Society of Photo-Optical Instrumentation Engineers (SPIE). [DOI: 10.1117/1.3575645]

Keywords: megavoltage scanning system (MVCT); near-infrared marker; motion tracking; total marrow irradiation.

Paper 10417R received Jul. 22, 2010; revised manuscript received Mar. 11, 2011; accepted for publication Mar. 21, 2011; published online May 00, 2011.

1 Introduction

As radiation therapy continues to advance, more conformal radiation treatment has been made possible. In conformal radiation treatment, the radiation dose conforms to the shape of the target while sparing sensitive neighboring areas of the body from high radiation delivery. Recently, total marrow irradiation is being explored as a part of the hematopoietic cell transplantation (HCT) preparative regimen.^{1–4} We have developed methodologies for selective total marrow irradiation (TMI) using tomotherapy,^{5,6} which has a potential to replace the current method of total body irradiation (TBI). Tomotherapy is an image guided radiation therapy machine that delivers conformed radiation helically around the patient. It has an onboard megavoltage computed tomography (MVCT) detector which supports 3D image guidance for patient setup.^{7–13} TMI treatment using tomotherapy is critically dependent on accurate patient positioning.^{14,15} During the development and initial clinical experiences of TMI treatment, we acknowledged potential challenges and concerns such as: a. risk of geographic miss if proper precautions are not taken during precise delivery, b. hour long treatment time, and c. the lack of “closed loop” technology that would provide feedback to the irradiation system notifying of an unsafe patient position so

as to disable the primary radiation beam to allow for adjustments to be made in the patient position during treatment.

Different strategies are used to monitor the patient's body motion between treatment fractions (interfraction) or during (intrafraction) treatment. One obvious strategy is to immobilize the patient using frame-based treatment such as an alpha cradle.^{16,17} Though immobilization techniques improve treatment delivery, they cannot be used to correct for various involuntary patient body movements during treatment such as breathing motion. Various methods have been proposed, investigated, and implemented to track patient (or surface) motion or target motion. These include x-ray tracking,¹⁸ electronic portal imaging,¹⁹ ultrasound tracking,²⁰ 4DCT,²¹ and camera-based optical tracking systems.^{22,23} These modalities in turn have inherent limitations such as ultrasound is limited to image soft tissue, and as a result would not be useful to track whole body. A predominant limitation of x-ray and 4DCT is the radiation exposure as even under optimal conditions they induce a dose per imaging session. The portal imaging being a two-dimensional (2D) projection method contains effects of superimposed structures between radiation source and detector. It shows large density differences as an example while distinguishing air and bone from soft tissue background. This poses a problem for tumor verification as most tumors are made of soft tissue. As such, the optical motion tracking system holds promise because it does not involve radiation exposure. Moreover, it is a noninvasive methodology that

Address all correspondence to: Susanta K Hui, University of Minnesota Medical School, Department of Therapeutic Radiology – Radiation Oncology, 420 Delaware Street SE, Mayo Mail Code 494, Minneapolis, Minnesota 55455. Tel: 612–626–4484, Fax: 612–626–7060, E-mail: huixx019@umn.edu

76 does not require surgical implants of fiducial markers and can
 77 be used to track the patient's whole body position, a necessity
 78 for ensuring the correct alignment of patients receiving TMI
 79 treatment.²³

80 Tracking multiple points on the body surface is an informa-
 81 tive method to know about the articulation of segments. Using
 82 the point tracking algorithm as a base, body segments such as
 83 boney anatomy, the head or the breastplate can be fairly well
 84 approximated as rigid bodies individually as they do not de-
 85 form much, but not with respect to each other. This method may
 86 be used to collect information about the location and orienta-
 87 tion of individual body parts throughout the treatment process,
 88 which may provide meaningful feedback to medical personnel
 89 to reposition patients. This manuscript aims to report the fea-
 90 sibility of a near-infrared (NIR) marker- based optical tracking
 91 system (OTS) to monitor body motion during highly confined
 92 TMI treatment. The present work describes: a. the calibration of
 93 NIR optical tracking system; b. the comparison of OTS with
 94 an onboard three-dimensional (3D) MVCT scanning system
 95 used for pre-treatment setup verification during TMI treatment;
 96 c. characterize the OTS to measure changes in the marker posi-
 97 tion associated with deep and normal breathing motion in human
 98 volunteers.

99 2 System Overview

100 In the present study, we used two different patient position-
 101 ing systems, the OTS and the onboard MVCT imaging system.
 102 Written below is a brief description of the two systems.

103 2.1 Optical Tracking System

104 2.1.1 OTS setup

105 The OTS consists of a spectroscopic camera system with NIR
 106 reflective markers obtained from Motion Analysis Corp. (MAC,
 107 Santa Rosa, California). Small rubber sphere markers with re-
 108 flective tape are attached to a rando phantom (The Phantom
 109 Laboratory, Salem, New York) [Fig. 1(a)] and human volun-
 110 teer [Fig. 1(b)] with an adhesive on the base. Each marker is a
 111 12.5-mm diameter spherical rubber ball painted with NIR re-
 112 flective powder. The cameras have a ring of light emitting diodes
 113 (LEDs) positioned around the lens. The NIR markers reflect the
 114 light from the LEDs back to the cameras. The cameras capture
 115 intensity images, which are then thresholded, and the centroid of
 116 each high-intensity connected region is found by a triangulation
 117 method. Each camera is calibrated (details given in Sec. 3.2.1)
 118 and the location of the center in each camera's image plane is
 119 used to determine the 3D location of the detected markers. The
 120 entire stereoscopic marker detection system returns a set of 3D
 121 marker locations at a rate of 60 Hz.

122 2.1.2 Motion data capture and analysis

123 The captured motion data is saved in the format of track row
 124 column (.trc) and hierarchical translation and rotation (.htr2)
 125 in the Eva real-time software (EVA^{RT}) (MAC, Santa Rosa,
 126 California). The .trc files containing translational motion data
 127 are in ascii format and can be imported into Microsoft Excel to
 128 allow basic editing which involves data cleaning and smoothing
 129 of the discontinued points. The position data for each marker is

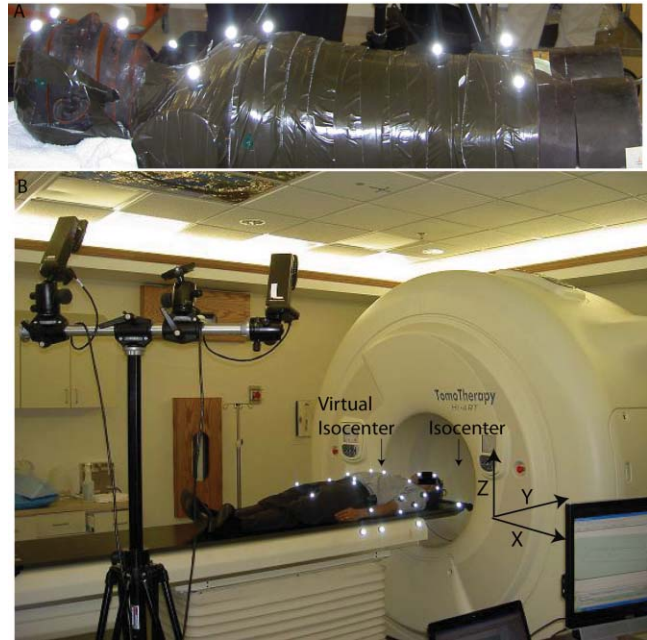


Fig. 1 An overview of the OTS. (a) Rando phantom with near-infrared markers. (b) Two of the six cameras used for tracking the infrared markers and a human volunteer to show the schematic representation.

organized into three columns per marker (X , Y , and Z position) with each row being a new frame. The position data is relative to the global coordinate systems of the capture volume and the position values are in the same units used for calibration.

134 2.2 Tomotherapy and the MVCT Imaging System

135 The Tomotherapy has a 6-MV linear accelerator mounted on a
 136 ring gantry to deliver radiation in a helical manner.^{24–26} The
 137 patient lies on the table which then moves through the rotating
 138 ring gantry. The tomotherapy uses the International Electrotech-
 139 nical Commission (IEC) gantry coordinate system (X , Y , Z) as
 140 shown in Fig. 1(b).^{24,27} During the treatment, the patient is
 141 placed on the Tomotherapy couch at the virtual isocenter taken
 142 at the intersection of the gantry axis with the axial CT slice
 143 containing the point of calculation. This is done for initial laser
 144 based alignment. For radiation delivery and MVCT image scans
 145 couch moves 70 cm into the bore (Y translation). After each
 146 image scan, the couch moves back to virtual isocenter position.
 147 In tomotherapy, a linear array of 738 xenon gas detectors and a
 148 radiation source with an average energy of 1.36 MeV are used to
 149 generate a 3D MVCT image with a field of view of 40 cm. Three
 150 different MVCT scanning modes, viz., fine, normal, and coarse,
 151 can be used to scan the patient with a slice thickness of 2, 4,
 152 and 6 mm, respectively. The treatment planning CT [kilovoltage
 153 computed tomographic (kVCT) image from the CT scanner] is
 154 superimposed on the MVCT images prior to radiation delivery.
 155 The rigid body image registration method is used to match two
 156 3D image sets (kVCT and MVCT) based on anatomical features
 157 and tumor locations.²⁸ The patient positioning errors acquired
 158 by the registration process are used in adjusting the patient to
 159 reduce day to day misalignment during radiation treatment.

3 Methods

Figure 2(a) shows a flowchart of total marrow irradiation process with anticipated addition to monitor real time body motion (bold). Figure 2(b) shows a flowchart of an OTS feasibility experiment. To track the motion changes in the rando phantom three series of experiments are conducted.

3.1 Calibration of the Optical Tracking System

An initial calibration of the NIR markers and the camera arrangement is done using a dynamic 3D calibration method. We use a wand with three markers arranged in a row at a known distance. The wand is moved around until the measurement space is covered which in the present study is the tomotherapy treatment couch. The combined field of view is calibrated by sweeping the wand in all possible directions while the spectroscopically arranged six cameras track the points on the wand. This process generally takes from a few seconds to a couple of minutes depending on the system's detailed requirements. In the present study, it took a few minutes to track a broader area (120×50 cm) covering the tomotherapy bench as shown in Fig. 1(b). The calibration of OTS involves measuring the deviations from known distances between the markers on the wand as measured by the cameras with the EVaRT. Using known distance values, an error approximation algorithm averages the position of each point based on the data gathered by each camera for each frame and calculates an error by which the cameras track a point. This is done for the total number of frames (frame frequency $n = 60$ Hz) used while collecting data on the wand movements, and then averaged. The collected data is analyzed in Microsoft Excel to determine standard deviation of the average error values for each frame. For further reference, this data will be referred to as optical data.

3.2 Measurement and Comparison of Translation Change in Marker Position

The parameters obtained from the calibration procedure (Sec. 3.1) are stored and used for the transformation of image coordinates into 3D marker coordinates. As a result, it is crucial to keep the cameras at the same position throughout the data collection. For evaluating the efficiency of the OTS in locating the position of NIR markers, we glued three NIR markers on the face of a rando phantom. As shown in Fig. 1(a), two markers are placed on the forehead to measure head motion and third marker is placed on the chin to measure motion in the lower jaw and mandible. Placement of three markers is designed to measure head and neck (H&N) skeleton movement. This design also helps to correct any misalignment in pitch (rotation along Y axis), commonly noticed during H&N patient localization for H&N cancer treatment. Without changing the spectroscopic arrangement of cameras, the rando phantom is positioned on the tomotherapy treatment bench. The various steps involved in the evaluation of the OTS are mentioned below.

3.2.1 Measurement of the initial location of markers

After aligning the rando phantom, the MVCT scan is performed three times (in three scanning modes viz. fine, normal, and coarse). Optical data is collected for each MVCT scan. This

optical data is stored as the reference optical data for the respective scanning mode. The other optical data collected in Secs. 3.2.2 and 3.2.3 is compared with this reference optical data.

3.2.2 Measurement of translational change in marker position

Next, in a series of trials, we manually shifted the rando phantom in a vertical direction by increasing the height of the couch (IEC + "Z direction") by $Z_{tr} = 10, 30,$ and 50 mm, where Z_{tr} is the translational shift in the vertical direction. For each position of the rando head we collected the OTS data and took three scans (fine, normal and coarse) as mentioned in Sec. 3.2.1.

3.2.3 Comparison of OTS and MVCT registration-based marker location systems

After each MVCT scan, we used the three in-built tomotherapy registration algorithms to determine the realigning corrections; bone, bone/tissue, and full image. In the bone and bone/tissue algorithms threshold values are respectively set to identify bone (i.e., pixels > 1.1 g/cm³) and bone/tissue (i.e., pixels > 0.3 g/cm³). The full image-based algorithm has no thresholding for the registration process. The OTS-based detection was repeated several times. Figure 2(d) shows a pictorial representation of the MVCT registration done for the face of the rando phantom. All the MVCT corrections are recorded. The optical data collected in Secs. 3.2.1 and 3.2.2 is compared with the MVCT image registration data.

3.3 General Tracking of the Markers

The point tracking algorithm used in the present OTS system works by correlating tracking identification numbers from one frame to the next. Essentially, the tracking number of the nearest point in the last frame is assigned to each point in the current frame. Defining $\ell_{(i,n)}$ to be the location of point i in the current frame and $\ell_{(j,n-1)}$ to be the location of some point j in the previous frame, the tracking identification number associated with $\ell_{(i,n)}$ tracks the identification number associated with the point in the previous frame satisfying $\min_j \{ \|\ell_{(i,n)} - \ell_{(j,n-1)}\|_2^2 \}$. Consistency checks are performed to make sure no identification number is assigned to more than one point in the current frame. If two or more points in the current frame are associated with a single point in the previous frame, only the closest point in the current frame will be associated with it. If a point does not correlate with any point in the previous frame, it is given a new tracking number. A threshold distance d_{thresh} is set for the maximum distance allowed for a point in the current frame to correlate with a point in the previous frame. This value is based upon the expected movement of points between frames. Thus, a point $\ell_{(i,n)}$ will not correlate with any points in the previous frame if $\min_j \{ \|\ell_{(i,n)} - \ell_{(j,n-1)}\|_2^2 \} > d_{\text{thresh}}$. In addition, points that disappear are propagated in their current location for a short duration of time, in the hope that they will reappear shortly. This is done to prevent losing points that temporarily disappear due to a momentary hiccup in the marker detection system. A threshold is manually set as to how many frames a point should be thus propagated since it has last been seen.

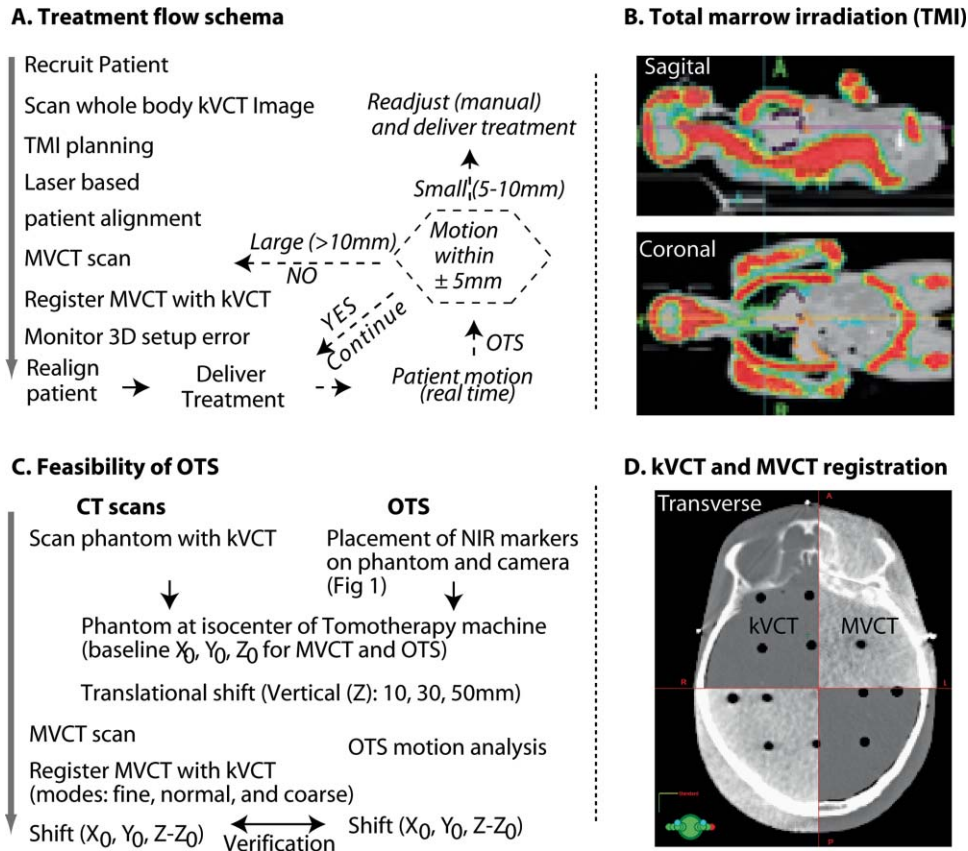


Fig. 2 (a) Treatment schema. Bold (with dotted line) is anticipated integration of real time monitoring of patient body motion for TMI radiation treatment delivery. (b) Validation of OTS system compared with MVCT to measure translation shift of known displacement. (c) The kVCT (dark grey) and MVCT image (light gray) registration of the rando head.

Q1

268 To track body segments such as boney anatomy, the rigid
 269 bodies tracked must be manually defined by an operator on captured
 270 data sets. A set of points are chosen for each rigid body in an initial
 271 frame, which are then tracked with any tracking system such as the OTS
 272 system. A rigid body in three dimensions contains six degrees of freedom.
 273 The three-dimensional location of the rigid body, $\mathbf{x} = (x, y, z)^T$, is found by
 274 taking the mean location of the points associated with it. The locations of
 275 each of the constituent points are then found with respect to this center
 276 location. Rotation is described by an angle of rotation, θ , and a unit
 277 vector around which rotation takes place, $\mathbf{r} = (r_x, r_y, r_z)^T$ in which
 278 $\|\mathbf{r}\| = 1$. The Levenberg–Marquardt minimization algorithm is then used
 279 to find the best quantities for the set of values $\{x, y, z, r_x, r_y, r_z, \theta\}$
 280 by minimizing the errors between the expected location of the object
 281 points and the detected location of these points within the scene. The
 282 Levenberg–Marquardt algorithm is a good choice because the bodies being
 283 tracked are not perfectly rigid, but minimum error approximations can
 284 still be found.

287 3.4 Breathing Motion Analysis Experiment

288 To track changes in the body surface as a result of breathing motion,
 289 we collected breathing motion data from two human volunteers. A set of
 290 16 NIR markers are placed on the chest in a 4×4 mesh like the
 291 arrangement shown in Fig. 3. The distance

292 between neighboring NIR markers is kept approximately 10 cm. This
 293 creates a 4×4 mesh of roughly 40×40 cm dimension. The markers
 294 cover longitudinally most of the chest width-wise and vertically from
 295 thoracic to the top of the abdominal surface of the diaphragm. The NIR
 296 marker position data is collected for slow and deep breathing motion.
 297 The volunteers are asked to hold their breath for a few seconds. The
 298 optical data collected during breath hold is taken as reference data
 299 (B_{ref}). Volunteers are then told to start the breathing first at normal
 300 rate (B_{normal}) and then at deep breathing rate (B_{deep}). During this
 301 procedure most of the other motions were controlled by placing the
 302 volunteers in an alpha cradle immobilization device. The OTS system
 303 records the NIR marker position as the volunteer breathes. The
 304 magnitude of normal and deep breathing depends on the comfort level
 305 of volunteers. In order to create smooth transitions between different
 306 breathing cycles, the human volunteers are asked to perform 2 to 3
 307 min breathing motions. This covers small variations in the breathing
 308 process. The noise from in the recorded .trc and .htr2 files are removed
 309 and discontinued points are smoothed.

312 4 Results

313 The calibration of OTS is done with a dynamic linearization technique
 314 using the 3 point wand. The Motion Analysis Inc. optical tracking
 315 system has been widely used for scientific and

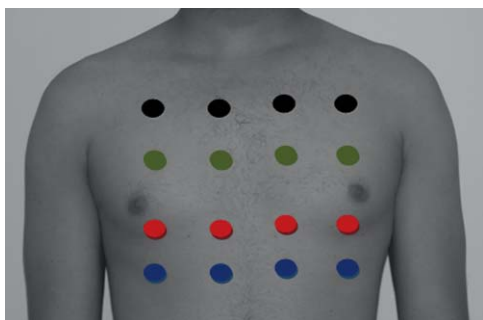


Fig. 3 Pictorial representation of 16 NIR markers placed on a human chest surface to track the breathing motion changes. Different colors are used to distinguish the location of markers.

316 technical purposes, and reliability and validity has been est-
 317 ablished and reported in literature.²⁹ In the present calibra-
 318 tion measurements, the average spatial error in locating the
 319 NIR marker position is 0.36 mm with a standard deviation of
 320 0.19 mm.

321 The image registration (as shown in Fig. 2) is done first
 322 by using an automatic method followed by a manual check.
 323 This is a double check to verify alignment of the MVCT and
 324 kVCT images. The shift in XYZ coordinates needed to align
 325 the MVCT image to the kVCT image is recorded. The NIR
 326 marker position changes during the translational motion of the
 327 rando phantom in the vertical (z) direction are compared with the

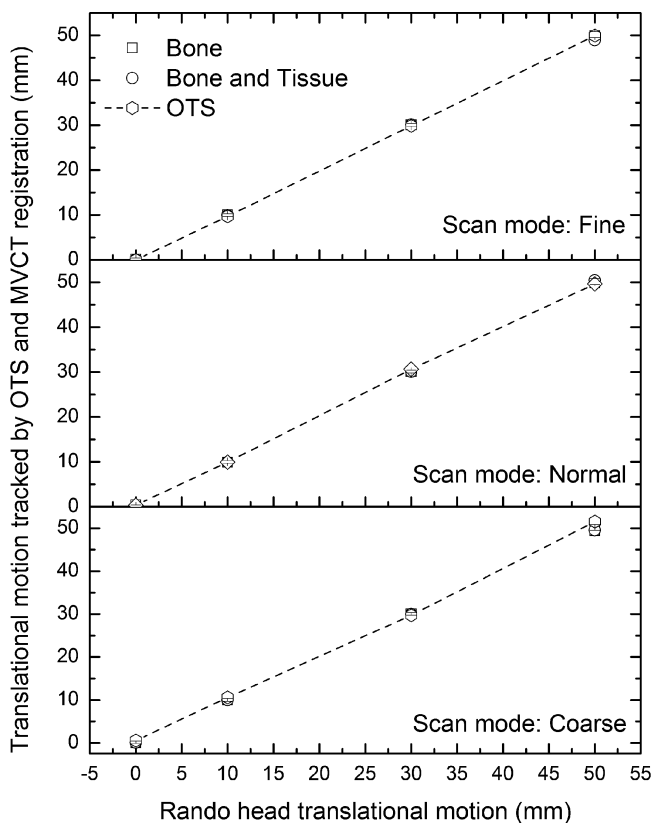


Fig. 4 Tracking translational changes in Z using the OTS and MVCT registration methods—bone, bone, and tissue and three different scanning modes—fine, normal and coarse.

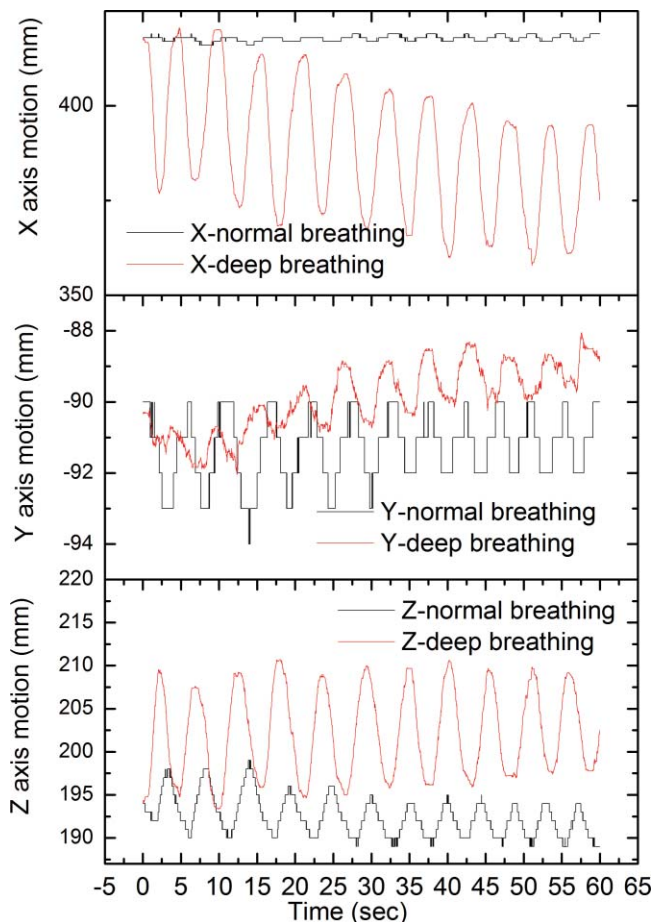


Fig. 5 Breathing motion changes in one marker in the X, Y, and Z directions with respect to time.

OTS system detection uncertainties in Fig. 4 for three scanning 328
 modes (fine, normal, and coarse) and two MVCT registration 329
 algorithms (bone and bone/tissue). The OTS system shows an 330
 uncertainty of ~ 1.5 mm in the detection of translation shifts 331
 in the rando head. The maximum uncertainty in the detection by 332
 the MVCT scanning modes is ~ 2 mm in the case of coarse mode. 333
 Better detection accuracy (0.5 to 1.0 mm) is found in fine and 334
 normal scanning modes. The average deviation and maximum 335
 percentage difference between three registration algorithms are 336
 0.35 mm and 1.9% in the case of the fine scanning mode and 337
 0.34 mm and 1.2% in the case of the normal scanning mode. 338
 In the case of the coarse scanning mode, the average deviation 339
 is 0.35 mm and maximum percentage difference between three 340
 registration algorithms is 6.8%. For a given registration method, 341
 the coarse scanning mode reduces the scanning time but it might 342
 compromise the measurement accuracy when the structures are 343
 small. 344

345 We observed the breathing motion changes in the case of two
 346 human volunteers. Figure 5 shows the normal and deep breath-
 347 ing motion for time = 1 min in the XYZ coordinates measured
 348 by one NIR marker. As seen in Fig. 5, each breathing cycle
 349 is from 5 to 7 s. The OTS is found to be capable of tracking
 350 the correlation between the timing of maximum inspiration and
 351 expiration time points. To better visualize the changes in NIR
 352 marker position of all 16 markers, we plotted the 3D position and

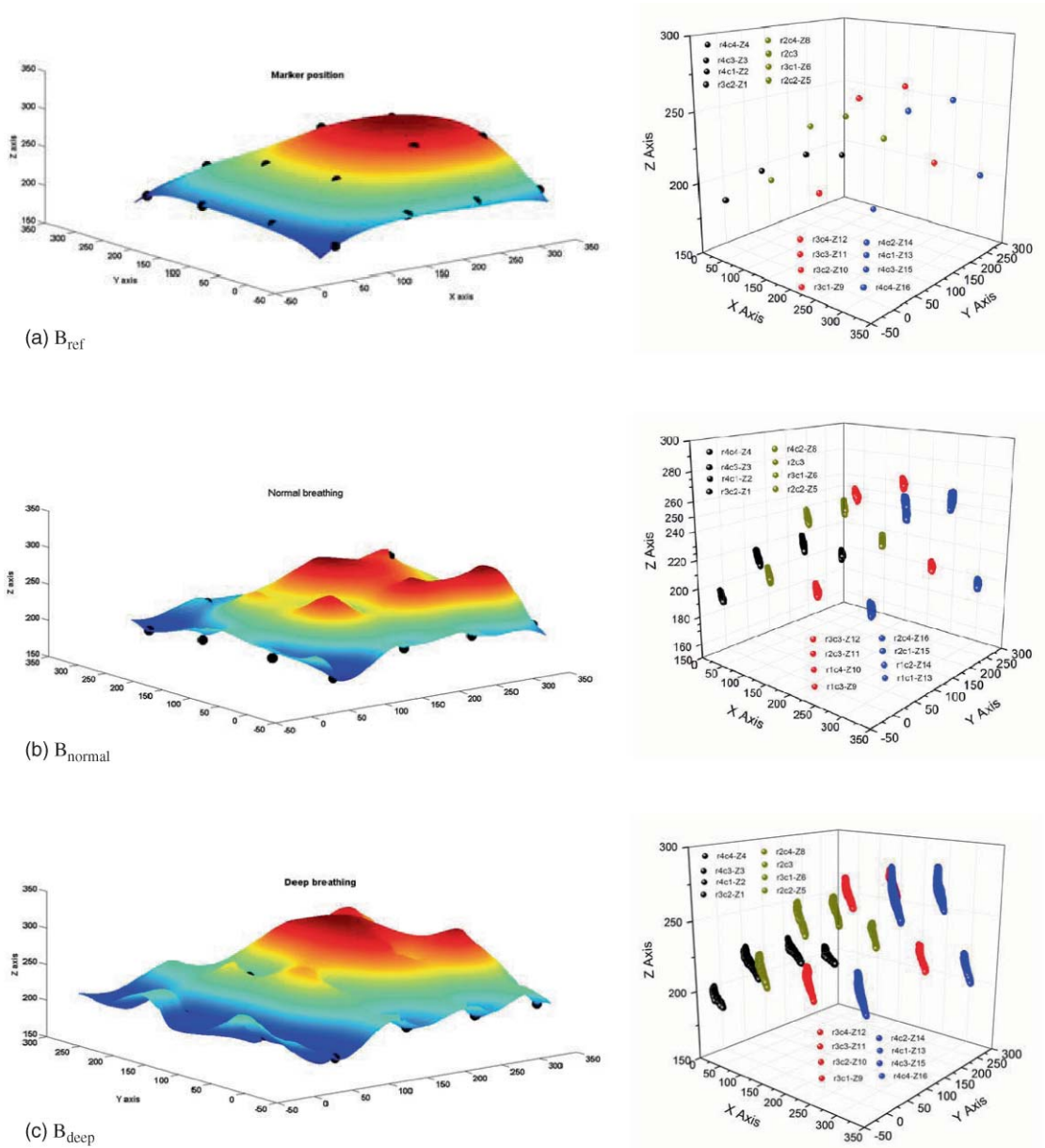


Fig. 6 Surface and 3D scatter plot of change in the position of 16 NIR markers placed on the chest surface of a human volunteer during. (a) the rest phase (B_{ref}); (b) normal breathing (B_{normal}); and (c) deep breathing (B_{deep}).

353 surface graphs in Figs. 6(a), 6(b), and 6(c), respectively, showing B_{ref} , B_{norm} , and B_{deep} . By keeping the initial position of the markers, the surfaces are constructed for B_{ref} , B_{norm} , and B_{deep} using the grid data and mesh functions of MATLAB (MATLAB 2007b, The Mathworks Inc., Natick, Massachusetts). The grid data function is used with the v4 method. The v4 method uses a Green's function approach and uses a full matrix composed of all the inter point distances to produce smooth surfaces. A 3D scatter plot graph is drawn using Microcal Origin Pro 8.0 (Microcal Software Inc., Northamtom, Masscuhsetts). As shown in Fig. 6, the markers placed near the top of the abdominal surface of the diaphragm show a larger magnitude of change in marker position compared to the markers placed near the mid-thorax and apex. In the case of normal breathing, the maximum shifts in the marker position coordinates in the X, Y, and Z directions

are, respectively, 2, 1, and 4 mm. In the case of deep breathing, the maximum changes in X, Y, and Z marker coordinates are respectively, 7, 3, and 12 mm, respectively.

5 Discussion

The feasibility of an NIR marker-based optical tracking system has been demonstrated to monitor rigid and dynamic motion in phantom and in two human volunteers using a tomotherapy treatment unit. The OTS is found to detect changes on par with those of the currently used MVCT scan-based method. The NIR markers used in the present study are equally efficient in light and dark environments compared to the infrared markers, which have a high noise level in light. The current results indicate that OTS should perform well enough to reliably detect 1.5 mm

381 movement for the human phantom. To get better target position-
 382 ing accuracy with image registration the fine or normal scanning
 383 modes should be used. The use of OTS in tracking patient mo-
 384 tion changes during treatment is beneficial in many respects.
 385 The OTS may be used in real time while treatment is underway
 386 (Fig. 2) and issue alerts if a patient moves significantly; a capabil-
 387 ity that is not currently present. The on-line approach of the im-
 388 age registration process in tomotherapy prolongs the overall total
 389 treatment time when compared to conventional treatments.³⁰ In-
 390 creased radiation exposure from multiple MVCT scans, prolong
 391 treatment time to incorporate MVCT scans, and its inability to
 392 measure real time body motion limits its application in TMI
 393 treatment. Due to a narrow field of view (40 cm), often MVCT
 394 is not useful to scan extremities (for example, arms) for adult
 395 patients. On the other hand, the vision-based acquisition can be
 396 performed for the entire body in real time very quickly (within
 397 a minute) compared to the MVCT scan method (scanning time
 398 > 30 min for whole body scan). The human body is capable of
 399 moving into many different positions. As such, it is important to
 400 know the extent of movement in different directions. With the
 401 OTS it is feasible to track the portions of the body (such as the
 402 head and chest) separately. This system will provide information
 403 about the alignment for each body portion for the patient's en-
 404 tire body as opposed to monitoring the motion of a small tumor
 405 region (few centimeters).^{22,23}

Q2

406 Lung toxicity is considered a primary dose-limiting factor for
 407 TBI due to increased dose to lungs.³¹ One of the main aims for
 408 the recently developed total marrow irradiation (TMI) method
 409 is to reduce radiation dose to lungs to control lung toxicity.^{5,6,32}
 410 At present, safety margins around the thoracic bone are kept the
 411 same (approximately 1.5 cm) for all directions because of lim-
 412 ited knowledge of the directional chest wall motion. Breathing
 413 motion data shows a relatively larger variation in the diaphragm,
 414 in comparison to the apex and thoracic regions of the chest.
 415 A reduced safety margin in the apex and thoracic region may
 416 help to reduce radiation dose to the lungs. In the present ex-
 417 periment, we used 16 markers. For 3D lung motion, 58 markers
 418 have been considered for reasonable accuracy in estimating lung
 419 volume.³³ In the future, 3D chest wall motion measured by the
 420 markers will be correlated with variation in lung volume during
 421 the breathing cycle using a recently developed 4D CT scanner.
 422 Future development will also include the ability to optimize
 423 a number of parameters associated with the NIR markers (for
 424 example, spatial distance between markers and number of mark-
 425 ers) to monitor the whole body motion including pelvis, lower
 426 torso, and extremities of the body. An integrated system with
 427 automated detection of body motion, feedback to control moni-
 428 tor, and subsequent adjustment of patient or treatment delivery
 429 will improve the accuracy of the TMI radiation dose delivery
 430 and enhance safety of the treatment delivery. In our clinical
 431 TMI treatment, measured rotational shift (by the MVCT-kVCT
 432 registration) was less than 1°. Therefore, we have not initiated
 433 rotational verification. However, rotational motion will be stud-
 434 ied in the future.

435 We have shown the applicability of the OTS system in track-
 436 ing changes in rigid and dynamic systems. The OTS system can
 437 capture task specific dynamic information and allows extract-
 438 ing a great number of measurements long after the subject has
 439 moved. This method can be extended to track other anatomical
 440 features such as upper and lower body extremities includ-

441 ing arms. The next phase of the project will be able to detect
 442 natural features on the patient. Possibilities include use of the
 443 scale invariant feature transfer (SIFT),³⁴ speed-up robust fea-
 444 ture (SURF),³⁵ or other similar features. In addition, coughing
 445 or hyperventilation events will also be detected by using a laser
 446 source mounted above the patient's abdomen, which provides
 447 positional values of the abdominal cross section. Hyperventila-
 448 tion differs from coughing in terms of the displacement of the
 449 abdomen. It is possible that a patient maintain the same levels of
 450 displacement while hyperventilating, thus the only way to differ-
 451 entiate between normal breathing and hyperventilation is based
 452 on the frequency of breathing. For hyperventilation detection,
 453 therefore, a filter will be used which emphasizes frequencies
 454 above the fundamental breathing frequency of normal breath-
 455 ing, so that if the fundamental frequency drifts to a higher value,
 456 which is characteristic of hyperventilation, a detection will be
 457 issued. This muscle-movement tracking setup will generate tem-
 458 poral data providing information about points on the abdomen
 459 undergoing displacement during the breathing cycle. Tracking
 460 these points over time will help us monitor breathing and detect
 461 an anomaly during the course of monitoring. A multistage filter-
 462 ing scheme will be used to reduce an inherent noise in the laser
 463 data measurements. A spatial smoothing filter is first applied,
 464 in which the values of the nearby points in the same horizontal
 465 line are averaged. This is based on the notion of smoothness of
 466 the patient's abdominal cross section, and emphasizes the fun-
 467 damental breathing frequency of the patient while eliminating
 468 high frequency noise.

6 Conclusions 469

470 A noninvasive vision-based optical tracking system is shown
 471 to be a feasible option or a second check for measuring body
 472 motion within 1.5 mm accuracy and was validated using a 3D
 473 MVCT imaging system. Accurate assessment of lung motion in
 474 different directions may help to develop patient specific safety
 475 margins for radiation treatment delivery. Properly optimized
 476 optical tracking systems may be used to monitor whole body
 477 motion during TMI treatment delivery to increase accuracy of
 478 treatment delivery and reduce radiation dose to lungs.

Acknowledgment 479

480 This research was supported by the National Science Founda-
 481 tion (NSF No. CNS-0821474), the Digital Technology Center,
 482 and the Medical device grant at the University of Minnesota.
 483 This work was also supported by PHS Cancer Center Support
 484 Grant No. P30 CA77398. The authors thank Motion Analysis
 485 Corporation for providing the motion tracking cameras.

References 486

- 487 1. J. Wong, J. Rosenthal, A. Liu, T. Schultheiss, S. Forman, and
 488 G. Somlo, "Image-guided total-marrow irradiation using helical to-
 489 motherapy in patients with multiple myeloma and acute leukemia un-
 490 dergoing hematopoietic cell transplantation," *Int. J. Radiat. Oncol.,*
 491 *Biol., Phys.* **73**(1), 273–279 (2009).
- 492 2. I. J. Lee, J. Seong, C. G. Lee, Y. B. Kim, K. C. Keum, C. O. Suh, G.
 493 E. Kim, and J. Cho, "Early clinical experience and outcome of helical
 494 tomotherapy for multiple metastatic lesions," *Int. J. Radiation Oncology*
 495 *Biol. Phys.* **73**(5), 1517–1524 (2009).

Q3

- 495 3. J. Wilkie, H. Tiryaki, B. Smith, J. Roeske, J. Radosevich, and B.
496 Aydogan, "Feasibility study for linac-based intensity modulated total
497 marrow irradiation," *Med. Phys.* **35**(12), 5609–5618 (2008).
- 498 4. J. Wong, A. Liu, T. Schultheiss, J. Rosenthal, S. Forman, and G. Somlo,
499 "Reduced acute toxicities with image guided targeted marrow irradi-
500 ation (tmi) using helical tomotherapy (ht) in patients with multiple
501 myeloma and acute leukemia undergoing hematopoietic cell trans-
502 plantation (HCT)," *Int. J. Radiat. Oncol., Biol., Phys.* **69**(3S), 17–18
503 (2007).
- 504 5. S. Hui, J. Kapatoes, J. Fowler, D. Henderson, G. Olivera, R. Manon,
505 B. Gerbi, T. Mackie, and J. Welsh, "Feasibility study of helical tomother-
506 apy for total body or total marrow irradiation," *Med. Phys.* **32**(10),
507 3214–3224 (2005).
- 508 6. S. Hui, M. Verneris, P. Higgins, B. Gerbi, B. Weigel, S. Baker, C. Fraser,
509 M. Tomblyn, and K. Dusenbery, "Helical tomotherapy targeting total
510 bone marrow-First clinical experience at the University of Minnesota,"
511 *Acta Oncol.* **46**(2), 250–255 (2007).
- 512 7. S. K. Hui, R. K. Das, J. Kapatoes, G. Oliviera, S. Becker, H. Odau, J. D.
513 Fenwick, R. Patel, R. Kuske, M. Mehta, B. Paliwal, T. R. Mackie, J. F.
514 Fowler, and J. S. Welsh, "Helical tomotherapy as a means of delivering
515 accelerated partial breast irradiation," *Technol. Cancer Res. Treat.* **3**(6),
516 639–646 (2004).
- Q4 517 8. R. Jeraj, T. R. Mackie, J. Balog, G. Olivera, D. Pearson, J. Kapatoes,
518 K. Ruchala, and P. Reckwerdt, "Radiation characteristics of helical
519 tomotherapy," *Med. Phys.* **31**(2), 396–404 (2004).
- 520 9. J. M. Kapatoes, G. H. Olivera, J. P. Balog, H. Keller, P. J. Reckwerdt, and
521 T. R. Mackie, "On the accuracy and effectiveness of dose reconstruction
522 for tomotherapy," *Phys. Med. Biol.* **46**(4), 943–966 (2001).
- 523 10. T. R. Mackie, T. Holmes, S. Swerdloff, P. Reckwerdt, J. O. Deasy,
524 J. Yang, B. Paliwal, and T. Kinsella, "Tomotherapy: a new concept for
525 the delivery of dynamic conformal radiotherapy," *Med. Phys.* **20**(6),
526 1709–1719 (1993).
- 527 11. K. J. Ruchala, G. H. Olivera, J. M. Kapatoes, E. A. Schloesser, P. J.
528 Reckwerdt, and T. R. Mackie, "Megavoltage CT image reconstruction
529 during tomotherapy treatments," *Phys. Med. Biol.* **45**(12), 3545–3562
530 (2000).
- 531 12. K. J. Ruchala, G. H. Olivera, E. A. Schloesser, and T. R. Mackie,
532 "Megavoltage CT on a tomotherapy system," *Phys. Med. Biol.* **44**(10),
533 2597–2621 (1999).
- 534 13. J. S. Welsh, M. Lock, P. M. Harari, W. A. Tome, J. Fowler, T. R. Mackie,
535 M. Ritter, J. Kapatoes, L. Forrest, R. Chappell, B. Paliwal, and M. P.
536 Mehta, "Clinical implementation of adaptive helical tomotherapy: a
537 unique approach to image-guided intensity modulated radiotherapy,"
538 *Technol. Cancer Res. Treat.* **5**(5), 465–479 (2006).
- 539 14. X. Li, X. Qi, M. Pitterle, K. Kalakota, K. Mueller, B. Erickson, D. Wang,
540 C. Schultz, S. Firat, and J. Wilson, "Interfractional variations in patient
541 setup and anatomic change assessed by daily computed tomography,"
542 *Int. J. Radiation Oncology Biol. Phys.* **68**(2), 581–591 (2007).
- Q5 543 15. T. Bortfeld, S. Jiang, and E. Rietzel, *Effects Of Motion On The Total*
544 *Dose Distribution*, pp. 41–51, Elsevier (2004).
- 545 16. C. B. Saw, R. Yakoob, C. A. Enke, T. P. Lau, and K. M. Ayyangar,
546 "Immobilization devices for intensity-modulated radiation therapy
547 (IMRT)," *Med. Dosim.* **26**(1), 71–77 (2001).
- Q6 548 17. M. J. Murphy and J. Y. Jin, "Patient Immobilization and Movement,"
549 *Spine Radiosurgery* **35** (2008).
- 550 18. P. Keall, V. Kini, S. Vedam, and R. Mohan, "Motion adaptive x-ray
551 therapy," *Physics in Medicine and Biology* **46**(1), 1–10 (2001).
- 552 19. W. van Elmpt, L. McDermott, S. Nijsten, M. Wendling, P. Lambin,
553 and B. Mijnheer, "A literature review of electronic portal imaging for
554 radiotherapy dosimetry," *Radiother. Oncol.* **88**(3), 289–309 (2008).
- 555 20. A. Hsu, N. Miller, P. Evans, J. Bamber, and S. Webb, "Feasibility
556 of using ultrasound for real-time tracking during radiotherapy," *Med.*
557 *Phys.* **32**(6), 1500–1512 (2005).
- 558 21. T. Zhang, W. Lu, G. Olivera, H. Keller, R. Jeraj, R. Manon, M. Mehta,
559 T. Mackie, and B. Paliwal, "Breathing-synchronized delivery: a poten-
560 tial four-dimensional tomotherapy treatment technique," *Int. J. Radiat.*
561 *Oncol., Biol., Phys.* **68**(5), 1572–1578 (2007).
- 562 22. J. Wilbert, J. Meyer, K. Baier, M. Guckenberger, C. Herrmann, R. Hess,
563 C. Janka, L. Ma, T. Mersebach, and A. Richter, "Tumor tracking and
564 motion compensation with an adaptive tumor tracking system (ATTS):
565 System description and prototype testing," *Med. Phys.* **35**(9), 3911–
566 3921 (2008).
- 567 23. T. H. Wagner, S. L. Meeks, F. J. Bova, W. A. Friedman, T. R.
568 Willoughby, P. A. Kupelian, and W. Tome, "Optical tracking tech-
569 nology in stereotactic radiation therapy," *Med. Dosim.* **32**(2), 111–120
570 (2007).
- 571 24. T. R. Mackie, J. Balog, K. Ruchala, D. Shepard, S. Aldridge, E. Fitchard,
572 P. Reckwerdt, G. Olivera, T. McNutt, and M. Mehta, "Tomotherapy,"
573 in *Radiation Therapy Treatment Optimization* pp. 108–117, Elsevier
574 (1999).
- 575 25. J. N. Yang, T. R. Mackie, P. Reckwerdt, J. O. Deasy, and B. R. Thomad-
576 sen, "An investigation of tomotherapy beam delivery," *Med. Phys.*
577 **24**(3), 425–436 (1997).
- 578 26. J. Balog, T. R. Mackie, D. Pearson, S. Hui, B. Paliwal, and R. Jeraj,
579 "Benchmarking beam alignment for a clinical helical tomotherapy de-
580 vice," *Med. Phys.* **30**(6), 1118–1127 (2003).
- 581 27. J. P. Gibbons, K. Smith, D. Cheek, and I. Rosen, "Independent calcu-
582 lation of dose from a helical TomoTherapy unit," *J. Appl. Clin. Med.*
583 *Phys.* **10**(1), 103–119 (2009).
- 584 28. S. Boswell, W. Tomé, R. Jeraj, H. Jaradat, and T. R. Mackie, "Auto-
585 matic registration of megavoltage to kilovoltage CT images in helical
586 tomotherapy: an evaluation of the setup verification process for the
587 special case of a rigid head phantom," *Med. Phys.* **33**, 4395 (2006).
- 588 29. T. Svoboda, D. Martinec, and T. Pajdla, "A convenient multicamera
589 self-calibration for virtual environments," *Presence: Teleoperators &*
590 *Virtual Environments* **14**(4), 407–422 (2005).
- 591 30. P. Bijdekerke, D. Verellen, K. Tournel, V. Vinh-Hung, F. Somers,
592 P. Bieseman, and G. Storme, "TomoTherapy: Implications on daily
593 workload and scheduling patients," *Radiother. Oncol.* **86**(2), 224–230
594 (2008).
- 595 31. A. D. Volpe, A. J. M. Ferreri, C. Annaloro, P. Mangili, A. Rosso,
596 R. Calandrino, E. Villa, G. Lambertenghi-Deliliers, and C. Fiorino,
597 "Lethal pulmonary complications significantly correlate with individu-
598 ally assessed mean lung dose in patients with hematologic malignancies
599 treated with total body irradiation," *Int. J. Radiation Oncology Biol.*
600 *Phys.* **52**(2), 483–488 (2002).
- 601 32. S. K. Hui, M. R. Verneris, J. Froelich, K. Dusenbery, and J. S. Welsh,
602 "Multimodality image guided total marrow irradiation and verification
603 of the dose delivered to the lung, PTV, and thoracic bone in a patient: a
604 case study," *Technol. Cancer Res. Treat.* **8**(1), 23–28 (2009).
- 605 33. S. J. Cala, C. M. Kenyon, G. Ferrigno, P. Carnevali, A. Aliverti,
606 A. Pedotti, P. T. Macklem, and D. F. Rochester, "Chest wall and lung
607 volume estimation by optical reflectance motion analysis," *J. Appl.*
608 *Physiol.* **81**(6), 2680–2689 (1996).
- 609 34. H. Zhou, Y. Yuan, and C. Shi, "Object tracking using SIFT fea-
610 tures and mean shift," *Comput. Vis. Image Underst.* **113**(3), 345–352
611 (2009).
- 612 35. D. N. Ta, W. C. Chen, N. Gelfand, and K. Pulli, "SURFTrac: Efficient
613 tracking and continuous object recognition using local feature descrip-
614 tors," (2009).

Queries

Q1: AU: Please reword text of Fig. 2 without color words, as readers of print will see black and white figures.

Q2: AU: Please check change from “cms” to centimeters.”

Q3: AU: Please verify our edit of author list of Ref. 2.

Q4: AU: Please check Refs. 7, 13, 32, 33 and 35 for content errors, or provide the DOI.

Q5: AU: Please supply location of publisher for Ref. 15.

Q6: AU: Please supply correct journal title of DOI for Ref. 17, 18, 29, and 35.

Q7: AU: Please provide publisher location city/state for Ref. 15 and 24.